Antiferromagnetic metallic state in the heavily doped region of perovskite manganites

Y. Moritomo
PRESTO, JST, Japan
and CIRSE and Department of Applied Physics, Nagoya University, Nagoya 464-01, Japan

T. Akimoto and A. Nakamura
CIRSE and Department of Applied Physics, Nagoya University, Nagoya 464-01, Japan

K. Ohoyama and M. Ohashi
Institute for Materials Research, Tohoku University, Sendai 980-77, Japan

(Received 5 March 1998)

Comprehensive study on electronic and magnetic properties has been performed for doped manganite near the phase boundary of the antiferromagnetic metallic (AFM) state, with changing the nominal hole concentration x and the one-electron bandwidth W. In $La_{1-x}Sr_xMnO_3$ with maximal W, the ferromagnetic metallic ground state in the low-x region is replaced by the AFM state beyond $x=0.54$. On the other hand, the charge-ordered insulating (COI) state appears at $x\sim0.5$ for $Nd_{1-x}Sr_xMnO_x$ with reduced W. The COI ground state is overwhelmed by the AFM state with further increasing x ($\geqslant0.54$) or W. These competitions of the AFM state with the alternative ground states suggest that the AFM state is a fundamental ground state for doped manganites. [S0163-1829(98)02333-9]

I. INTRODUCTION

The recent observation of ''colossal'' magnetoresistance[1] (the CMR effect) in the doped manganites has sparked a great amount of effort to understand the unusual electronic and magnetic properties of these materials. The most commonly studied manganites $R_{1-x}A_xMnO_3$, where R and A are the trivalent rare-earth and divalent alkaline-earth ions, respectively, have the distorted perovskite structure with three-dimensional networks of the MnO_6 octahedra. Its generic behavior of paramaganetic-to-ferromagnetic transition is understood within the framework of double-exchange (DE) theory,[2–4] which includes only the transfer integral t of the e_g electrons and the on-site exchange interaction (Hund's-rule coupling J_H) between the itinerant e_g electrons and localized t_{2g} spins ($S=3/2$). To explain the ''colossal'' value of the magnetoresistance for the system having small W, however, we need an additional mechanism for carrier localization above T_C as well as magnetic-field release of the localization. Perhaps, the most probable mechanism to supplement the DE model is the polaron formation originating from the Jahn-Teller instability of the MnO_6 octahedra.[5]

The doped manganites show much more multifarious properties in the heavily doped region ($x\geqslant0.5$). In $Nd_{0.5}Sr_{0.5}MnO_3$,[6] a charge-ordered insulating (COI) state emerges below $T_{CO}=160$ K with the concomitant ferromagnetic-antiferromagnetic transition. Kawano *et al.*[7] have performed a systematic neutron-diffraction measurement for $Nd_{1-x}Sr_xMnO_3$. They have found that the spin ordering of the COI ground state at $x=0.50$ is of the CE type with the $2\sqrt{2}\times2\sqrt{2}\times2$ unit cell in the cubic perovskite setting,[8] while that for $x=0.55$ is of a layered type (A type). The A-type spin structure is commonly found in the heavily doped region of the perovskite manganites, e.g., $Pr_{0.5}Sr_{0.5}MnO_3$ (Ref. 7) and $La_{0.46}Sr_{0.54}MnO_3$.[9] Recently, Akimoto *et al.*[9] have systematically investigated the ground-state properties for the manganites as a function of nominal hole concentration (x) and the averaged ionic radius (r_R) of the rare-earth ion, and found that the phase diagram is dominated by the ferromagnetic metallic (FM) state in the low-x region and an antiferromagnetic metallic (AFM) state with A-type spin structure in the high-x region. The AFM state, or *spontaneous acquisition of two dimensionality*, has been ascribed to formation of a pseudo-two-dimensional $d_{x^2-y^2}$ band due to kinetic energy gain of the e_g electrons.

It should be noted that the layered-type spin structure is observed even in the layered manganites, $R_{2-2x}Sr_{1+2x}Mn_2O_7$ ($R=$ rare-earth ions). In this system, the MnO_2 sheets are separated by rocksalt layers and the MnO_6 octahedra form a two-dimensional (2D) network. Battle *et al.*[10] have reported a layered-type AF state for $NdSr_2Mn_2O_7$ ($x=0.50$) and $Nd_{1.1}Sr_{1.9}Mn_2O_7$ ($x=0.45$). Moritomo *et al.*[11,12] have investigated the ground-state properties for layered manganites, $(La_{1-z}Nd_z)_{2-2x}Sr_{1+2x}Mn_2O_7$, as a function of x and the Nd concentration z, and indicated that the heavily doped region of the phase diagram is dominated by the layered-AF state. This again strongly suggests that the layered-AF state is the alternative ground state for doped manganites, besides the FM state.

In this paper, we have investigated electronic and magnetic properties for perovskite manganites $R_{1-x}Sr_xMnO_3$ ($R=$ La and Nd) near the AFM phase boundary, with systematically changing x and W. We can control the one-electron bandwidth W by means of the hydrostatic and chemical pressure, that is, chemical substitution of the rare-earth ion R.[13] In a previous paper,[9] we have reported a global ground-state phase diagram for cubic manganites as a function of x and W, and discussed the origin of the AFM state. Here, we have concentrated our attention on the competition of the AFM state with the alternative ground states, i.e., the FM and COI states. In $La_{1-x}Sr_xMnO_3$ with maximal

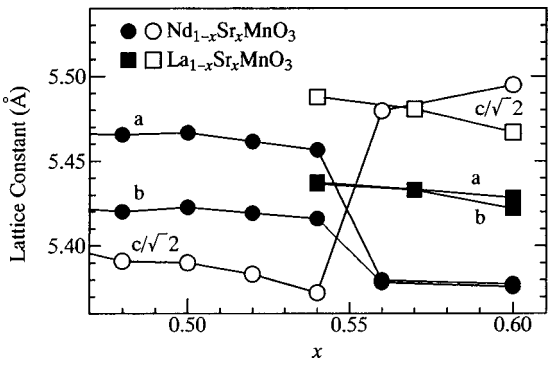

FIG. 1. Lattice constants for $La_{1-x}Sr_xMnO_3$ (squares) and $Nd_{1-x}Sr_xMnO_3$ (circles). The crystal symmetry is orthorhombic (*Pbnm*, $Z=4$).

one-electron bandwidth W of the e_g carriers, the FM state is replaced by the AFM state beyond $x=0.54$ from the low-temperature side. On the other hand, the COI state for $Nd_{1-x}Sr_xMnO_3$ is overwhelmed beyond $x=0.54$ from the high-temperature side. Application of hydrostatic or chemical pressure was found to suppress the COI state.

II. EXPERIMENT

Crystals of $R_{1-x}Sr_xMnO_3$ ($R=$La, Nd) were grown by the floating-zone method at a feeding speed of 7–9 mm/h. Stoichiometric mixture of commercial La_2O_3, Nd_2O_3, $SrCO_3$ and Mn_3O_4 powder was ground and calcined two times at 1350 °C for 24 h. Then, the resulting powder was pressed into a rod with a size of $\oslash 5\times 60$ mm and sintered at 1350 °C for 48 h. The ingredient could be melted congruently in a flow of O_2. Large crystals, typically 4 mm in diameter and 20 mm in length, were obtained. Powder x-ray-diffraction measurements at room temperature and Reitveld analysis[14] indicate that the crystals were almost single phase. A small amount of $SrMnO_3$ impurity phase, however, is inevitably introduced to the melt-grown crystal ingot, especially for the higher-x samples. Obtained lattice constants, a, b, and c are plotted in Fig. 1 in the orthorhombic ($Pbnm$, $Z=4$) setting. In $La_{1-x}Sr_xMnO_3$, the crystal symmetry changes from rhombohedral [$R\bar{3}c$, $Z=2$ (not shown)] to a psuedotetragonal one ($a\approx b\leqslant c$) beyond $x=0.54$. Similar pseudotetragonal structural is observed beyond $x=0.54$.

To investigate the magnetic structure, neutron-diffraction measurements were performed for $Nd_{0.48}Sr_{0.52}MnO_3$ ($x=0.52$) with a Kinken powder diffractometer for high-efficiency and high-resolution measurements, HERMES, installed at the JRR-3M reactor in Japan Atomic Energy Research Institute, Tokai, Japan. Neutrons with wavelength 1.819 Å were obtained by the (331) reflection of Ge monochromater, and 12′-∞-Sample-18′ collimation. Melt-grown crystal ingots were crushed into fine powder and were sealed in a vanadium capsule with helium gas, and mounted at the cold head of the closed-cycle He-gas refrigerator. The powder patterns are analyzed by the Rietvelt method,[14] and the obtained lattice parameters, a, b, and c are listed in Table I.

For four-probe resistivity measurements, the crystal was cut into a rectangular shape, typically of $3\times 1\times 0.5$ mm^3, and electrical contacts were made with a heat-treatment-type silver paint. Magnetization M was measured under a field of $\mu_0 H=0.5$ T after cooling down to 5 K in zero field using a superconducting quantum interference device magnetometer. Curie temperature T_C was determined from the inflection point of the M-T curve. Effects of an external hydrostatic pressure were measured using a clamp-type piston cylinder cell. A small piece of crystal ($\sim 0.5\times 1\times 2$ mm^3) was placed in the sample room, which was filled with silicone oil as a pressure transmitting medium. The sample temperature was monitored with a copper-constantan thermocouple placed in the sample room. According to our previous experience, it is inferred that beyond ~ 1 GPa the applied pressure relaxes at a rate of -8%/100 K, while the pressure relaxation effect is negligible ($\leqslant -2\%$/100 K) below 1 GPa.

III. RESULTS AND DISCUSSION

A. Electronic phase diagram

Before describing details for the competitions between the AFM state with the alternating ground states, e.g., FM state for $La_{1-x}Sr_xMnO_3$ or the COI state for $Nd_{1-x}Sr_xMnO_3$, let us survey the phase diagrams for doped manganites. In Fig. 2, we show the extended phase diagrams for (a) $La_{1-x}Sr_xMnO_3$ and (b) $Nd_{1-x}Sr_xMnO_3$. The data points above $x=0.5$ are determined in the present work, though those in the lightly doped region ($x\leqslant 0.5$) are cited from Ref. 13.

The phase diagram for $La_{1-x}Sr_xMnO_3$ [Fig. 2(a)] with maximal W is a canonical one for the DE system. The Jahn-Teller distorted state ($x\leqslant 0.1$) undergoes a phase transition to a spin canted insulating (CI) phase. A ferromagnetic insulating (FI) phase is present in a fairly narrow x region ($x=0.10$–0.17), in which the e_g carriers are subject to localization but can still mediate the ferromagnetic interaction between the neighboring sites. With further doping beyond $x\sim 0.17$, the FM phase appears in the low-temperature side. T_C steeply increases with x up to $x=0.3$ and then seems to saturate. With further increasing x beyond $x=0.54$, the AFM

TABLE I. Lattice constants and magnetic moments for $Nd_{0.48}Sr_{0.52}MnO_3$.

Temperature (K)	a (Å)	b (Å)	c (Å)	Magnetic structure	Moment (μ_B)	Direction
300	5.4207(3)	5.4632(3)	7.6151(4)	Paramagnetic		
220	5.4185(3)	5.4648(3)	7.5945(7)	Ferromagnetic	0.70(5)	[100]
180	5.4345(9)	5.4788(9)	7.5283(10)	A-type	0.80(5)	[100]
10	5.4388(11)	5.4898(12)	7.4999(13)	A-type CE-type	1.60(5)	[100]

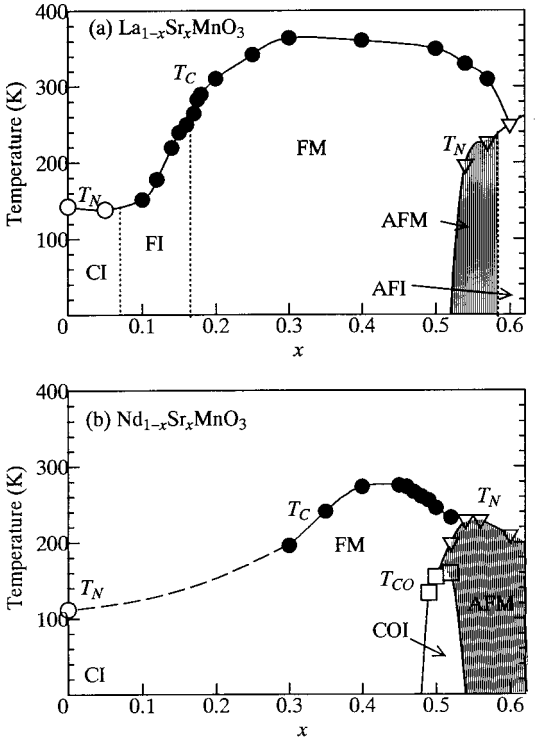

FIG. 2. Electronic phase diagram for (a) $La_{1-x}Sr_xMnO_3$ and (b) $Nd_{1-x}Sr_xMnO_3$. Filled circles, open triangles (circles), and open squares represent the critical temperatures for ferromagnetic (T_C), antiferromagnetic (T_N), and charge-ordering (T_{CO}) transitions, respectively. CI, FI, FM, AFM, AFI, and COI mean canted insulating, ferromagnetic insulating, ferromagnetic metallic, antiferromagnetic metallic, antiferromagnetic insulating, and charge-ordered insulating states, respectively.

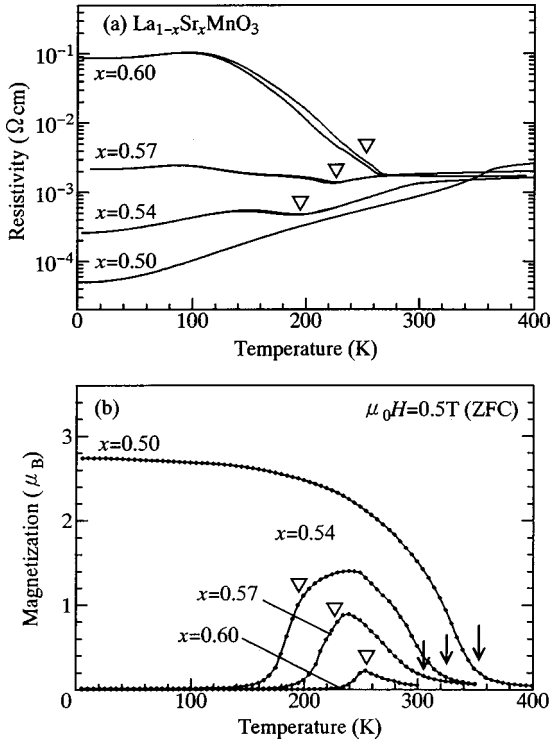

FIG. 3. Temperature dependence of (a) resistivity and (b) magnetization for $La_{1-x}Sr_xMnO_3$. Arrows and triangles represent the Curie temperatures (T_C) and Néel temperatures (T_N), respectively. Magnetization was measured under a field of 0.5 T after cooling down to 5 K in zero field (ZFC).

state appears.[9] The spin structure of this phase is of the A type with ferromagnetic sheets perpendicular to the crystallographic c axis.

Overall features of the phase diagram are similar for $Nd_{1-x}Sr_xMnO_3$ [Fig. 2(b)], though T_C is suppressed as compared with $La_{1-x}Sr_xMnO_3$ and begins to drop beyond $x \approx 0.4$. In the immediate vicinity of $x=0.5$, a charge-ordered insulating (COI) phase sets in below T_{CO} ($=160$ K).[6] The charge-ordering transition accompanies a ferromagnetic-to-antiferromagnetic transition. The low-temperature AF spin structure is of the CE type with the $2\sqrt{2}\times 2\sqrt{2}\times 2$ unit cell in the cubic perovskite setting.[8] The COI state is observed only in a limited x region and disappears below $x=0.48$. With further increasing x beyond $x=0.54$, the AFM state appears.[7,9,15] The A-type spin structure remains up to $x=0.62$.[17] Looking at Fig. 1, one may consider that the AFM state correlates to the structure with $c/\sqrt{2} \geq a,b$. We think, however, this trend is accidental. Becasue the transition into the AFM state accompanies significant compression of c (*vide infra*).

B. Competition between the FM and AFM states in $La_{1-x}Sr_xMnO_3$

The AFM state for $La_{1-x}Sr_xMnO_3$ is adjacent to the FM state. We show in Fig. 3 temperature dependence of resistivity ρ and magnetization M for $La_{1-x}Sr_xMnO_3$ in the vicinity of the AFM phase boundary. At $x=0.50$, the ρ-T curve steeply decreases below $T_C(=360$ K, downward arrow) down to $\sim 5\times 10^{-5}$ Ω cm at 5 K. By contrast, the $x=0.54$ crystal shows a ferromagnetic-antiferromagnetic transition at $T_N=200$ K. Nevertheless, the resistivity for $x=0.54$ remains low ($\sim 4\times 10^{-4}$ Ω cm at 5 K) even in the antiferromagnetic phase, indicating that the ground state is the AFM state. The metallic conductivity for $x=0.54$ is not due to the FM impurity, because the low-field magnetization curve of the same crystal piece as used for the resistivity measurement shows no ferromagnetic component. A similar FM-AFM transition is observed also for $x=0.57$. Here, we should emphasize that the ground-state spin structure is of the layered type, and hence the state can be viewed as a 2D FM state, while the usual FM state can be viewed as a 3D FM state. At $x=0.60$, ρ value steeply increases below $T_N=250$ K [antiferromagnetic insulating (AFI) state in Fig. 2(a)].

The key factor for realizing the AFM state is the anisotropy of the two e_g orbitals, i.e., the two-dimensional $d_{x^2-y^2}$ state and the one-dimensional $d_{3z^2-r^2}$ state. In the heavily doped region, the e_g-electron system gains the maximum kinetic energy when the $d_{x^2-y^2}$ orbitals form a pseudo-2D band. If such a pseudo-2D band were realized, the in-plane exchange interaction would be ferromagnetic mediated by the itinerant $d_{x^2-y^2}$ electrons (DE interaction), while the antiferromagnetic superexchange interaction should dominate along the z direction. In this sense, the origin of the in-plane ferromagnetic exchange interaction in the AFM state is qualitatively different from that for the parent material $LaMnO_3$ ($x=0.0$), in which in-plane ferromagnetic order-

ing is caused by the superexchange interaction between the neighboring e_g electrons that occupy the alternating e_g orbitals. The ordered moment shows no canting in the AFM state, which again makes a sharp contrast with the CI state for $LaMnO_3$. With decreasing x, the 2D AFM ground state is replaced by the 3D FM state, as shown in Fig. 2(a). The probable driving forces of the AFM-FM transition induced by the *electron doping* are (a) JT instability inherent to the Mn^{3+} (d_4) ions and (b) ferromagnetic superexchange interaction between the Mn^{3+} ions, both of which unstabilize the $d_{x^2-y^2}$ orbital.

It should be noted that the AFM transition accompanies a significant lattice deformation. For example, the lattice constant c shrinks more than 1% at the FM-AFM transition for $(La_{0.5}Nd_{0.5})_{0.5}Sr_{0.5}MnO_3$,[13] which is advantageous to formation of the pseudo-2D band. A similar compression of $c(\approx 1\%)$ is observed at the AFM transition for $Nd_{0.48}Sr_{0.52}MnO_3$ (see Table I). Thus, the e_g electrons gain the kinetic energy with forming the pseudo-2D band at the cost of the lattice energy. On the other hand, the lattice deformation is rather small in the FM transition as compared with that in the AFM transition. Even the elongation of c is observed at the FM transition for $(Nd_{0.06}Sm_{0.94})_{0.5}Sr_{0.5}MnO_3$ ($T_C = 120$ K).[16] Accordingly, the two metallic ground states, i.e., the AFM and FM states, prefer the different lattice deformations, which prevents the two magnetic structures from mixing. This forms a pronounced contrast with competitions between the COI and AFM states for $Nd_{1-x}Sr_xMnO_3$, in which the two magnetic structures are mixed (*vide infra*).

C. Competition between COI and AFM states in $Nd_{1-x}Sr_xMnO_3$

In the narrow-W compound like $Nd_{1-x}Sr_xMnO_3$, the COI state intrudes between the two ground states, i.e., the FM and AFM states, as shown in Fig. 2(b). Figure 4 shows prototypical examples for the (a) FM, (b) COI, and (c) AFM states for $Nd_{1-x}Sr_xMnO_3$. At $x = 0.40$ [Fig. 4(a)], the ρ-T curve steeply decreases below $T_C(=280$ K; downward arrow). Similarly, the $x = 0.5$ [Fig. 4(b)] crystal becomes a conducting ferromagnet below $T_C = 255$ K. With further lowering temperature, however, the charge-ordering transition takes place below $T_{CO} = 160$ K (square) accompanying a ferromagentic-antiferromagnetic transition. The spin structure of the COI ground state is of the CE type. Similarly to the case of the AFM transition, the charge-ordering transition accompanies a compression of c by $\approx 1.5\%$.[6] On the other hand, the ρ-T curve for $x = 0.6$ [Fig. 4(c)] remains metallic even below T_N (triangle) except for the low-temperature region (≤ 50 K), where the barely mobile e_g carrier is amenable to the Anderson localization effect. The spin structure of the AFM ground state is of the layered type (A type) perpendicular to the c axis.

The ρ-T curve for $Nd_{0.48}Sr_{0.52}MnO_3$ ($x = 0.52$; see thick curve in the upper panel of Fig. 5) is rather complicated. The ρ value gradually drops below $T_C = 230$ K (downward arrow), and then jumps below $T_N = 200$ K (triangle) accompanying a prominent thermal hysteresis. This resistivity jump accompanies a ferromagetic-antiferromagnetic transition (not shown). With further decreasing temperature, the ρ-T curve shows a slight rise around 150 K (square; compare with the ρ-T curve at $x = 0.54$), suggesting an antiferromagnetic-antiferromagnetic ordering transition. In Fig. 6 are shown the neutron powder patterns for $x = 0.52$: (a) 300 K$\geq T_C(=230$ K), (b) 220 K$\leq T_C$, (c) 180 K$\leq T_N(=200$ K), and (d) 10 K.

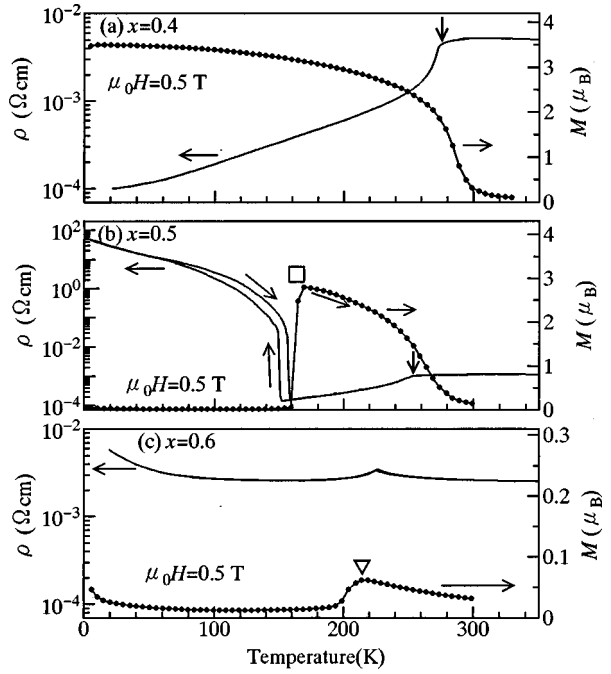

FIG. 4. Temperature dependence of resistivity and magnetization for $Nd_{1-x}Sr_xMnO_3$: (a) $x = 0.4$, (b) $x = 0.5$, and (c) $x = 0.6$. Arrows, squares, and triangles represent the Curie (T_C), charge-ordering (T_{CO}), and Néel (T_N) temperatures, respectively. Magnetization was measured in a field of 0.5 T after cooling down to 5 K in zero field (ZFC).

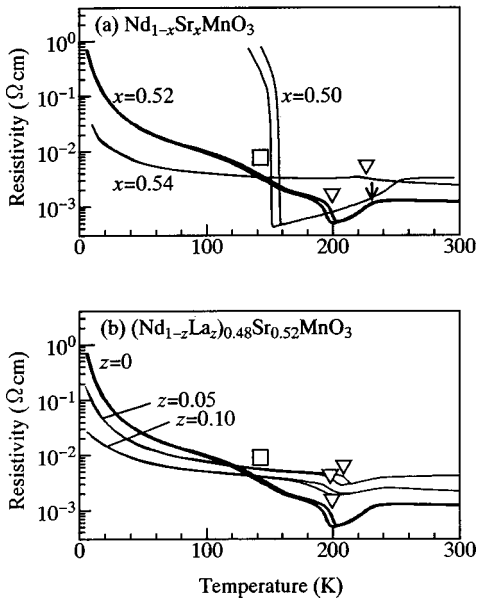

FIG. 5. (a) Filling-dependence and (b) chemical pressure effects of resistivity for $Nd_{1-x}Sr_xMnO_3$. Thick curve is for $Nd_{0.48}Sr_{0.52}MnO_3$ ($x = 0.52$). Downward arrows, squares, and triangles represent the ferromagnetic, antiferromagnetic, and charge-ordering transitions, respectively.

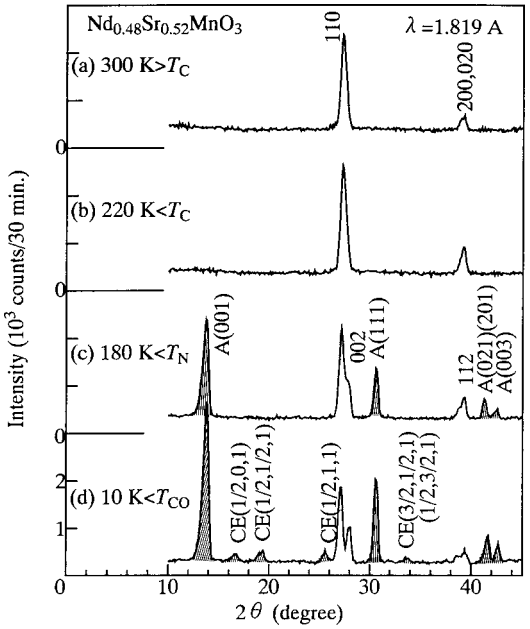

FIG. 6. Neutron powder profiles for $Nd_{0.48}Sr_{0.52}MnO_3$ ($x=0.52$) at various temperatures: (a) 300 K$\geqslant T_C$(=240 K), (b) 220 K$\leqslant T_C$, (c) 180 K$\leqslant T_N$(=210 K), and (d) 10 K$\leqslant T_{CO}$(=160 K). Shaded areas indicate magnetic reflections, which are indexed in the *Pbmn* setting. *A*, CE means that the reflection is originated in the *A*-type and CE-type antiferromagnetic structures, respectively.

In the ferromagnetic phase [see Fig. 6(b)], the magnetic reflections are overlapped on the nuclear reflections. The magnetic moment is estimated to be $(0.7\pm0.05)\mu_B$ by Rietveld refinement. On the other hand, magnetic superlattice reflections are observed below T_N [see Fig. 4(c)]. These reflections can all be indexed by the *A*-type structure. The parentheses are the indices of the magnetic reflections in the *Pbmn* setting. With further decreasing temperature, extra magnetic reflections appear. These can be indexed by the CE-type structure, indicating that the ground state is the charge-ordered state. Coexistence of the *A*-type and CE-type components causes the higher conductivity for $x=0.52$ as compared with $x=0.50$ (see Fig. 5). Concerning to the 180 K and 10 K pattern, we have estimated the magnitude and direction of the *A*-type component of the ordered moment. The results are listed in Table I.

With further hole doping, the COI ground state is replaced by the AFM state. Upper panel of Fig. 5 shows the x dependence of the ρ-T curve for $Nd_{1-x}Sr_xMnO_3$. The charge-ordering transition ($T_{CO}=160$ K) shows up as a steep rise of the resistivity for $x=0.50$. At $x=0.52$, the resistivity in the COI state (denoted by the square) significantly decreases down to $\sim10^{-2}$ Ω cm due to the *A*-type canting and resultant enhanced itineracy of the e_g carriers. The charge-ordering transition disappears for $x=0.54$, and the *A*-type spin structure remains down to the lowest temperature.

Application of the hydrostatic or chemical pressure (increase of W), which enhances the carrier itineracy, also suppresses the COI state. The lower panel of Fig. 5 shows W dependence of the ρ-T curve for $(Nd_{1-z}La_z)_{0.48}Sr_{0.52}MnO_3$, where the W value can be controlled by partial substitution of the larger La^{3+} ions for Nd^{3+} ions (z is the La concentration). The charge-ordering transition disappears at z

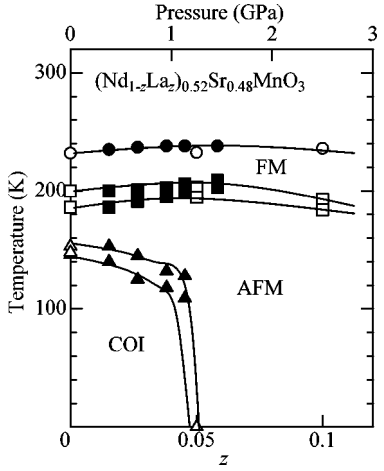

FIG. 7. Phase diagram for $(Nd_{1-z}La_z)_{0.48}Sr_{0.52}MnO_3$ ($x=0.52$) as a function of the La concentration. Filled symbols are the data points for $z=0.0$ obtained under hydrostatic pressure using a scaling relation that $z=0.04P$, where P is the compensated pressure value in units of GPa. FM, AFM, and COI mean ferromagnetic metallic, antiferromagnetic metallic and charge-ordered insulating states, respectively.

$=0.05$. In Fig. 7 are shown thus-obtained critical temperatures against z. Circles, squares, and triangles represent T_C, T_N, and T_{CO}, respectively. In the same phase diagram, we plotted the data points for $Nd_{0.48}Sr_{0.52}MnO_3$ ($x=0.52$, filled symbols) obtained under hydrostatic pressures using a scaling relation such that $z=0.04P$, where P is the calibrated pressure in units of GPa. The coefficient 0.04 is the same value as used in the phase diagram for $x=0.54$.[13] T_{CO} is suppressed and eventually disappear with increasing W, while T_C and T_N are insensitive to the W value.

IV. SUMMARY

Electronic and magnetic properties have been investigated for doped manganites near the phase boundary of the AFM state. In $La_{1-x}Sr_xMnO_3$, the FM state in the lightly doped region is replaced by the AFM state beyond $x=0.54$. On the other hand, in $Nd_{1-x}Sr_xMnO_3$, the COI state is overwhelmed by the AFM state with increasing x ($\geqslant0.54$) or W. In addition, the *A*-type (inherent to the AFM state) and CE-type (to the COI state) components coexist for $x=0.52$ near the COI-AFM phase boundary, causing a gradual doping-induced insulator-to-metal transition. This makes a sharp contrast with the FM-AFM phase boundary, in which the magnetic structure of the two metallic states cannot be mixed.

ACKNOWLEDGMENTS

The authors are grateful to H. Kawano, H. Kuwahara, and Y. Tokura for fruitful discussion, to K. Nemoto for his help in measurement of neutron powder patterns, and to T. Inami for his help in the analysis of the patterns. This work was supported by a Grant-in-Aid for Scientific Research from the Ministry of Education, Science, Sports and Culture, by Precursory Research for Embryonic Science and Technology (PRESTO), Japan Science and Technology Corporation (JST), and also by The Mazda Foundation Research Grant, Japan.

[1] For example, S. Jin, T. H. Tiefel, M. McCormack, R. Fastnacht, R. Ramesh, and L. H. Chen, Science **264**, 13 (1994).
[2] P. W. Anderson and H. Hasagawa, Phys. Rev. **100**, 675 (1955).
[3] P.-G. de Gennes, Phys. Rev. **118**, 141 (1960).
[4] N. Furukawa, J. Phys. Soc. Jpn. **63**, 3214 (1994); **64**, 2734 (1995); **64**, 2754 (1995); **64**, 3164 (1995).
[5] A. J. Millis, P. B. Littlewood, and B. I. Shraiman, Phys. Rev. Lett. **74**, 5144 (1994); **77**, 175 (1996).
[6] H. Kuwahara, Y. Tomioka, A. Asamitsu, Y. Moritomo, and Y. Tokura, Science **270**, 961 (1995).
[7] H. Kawano, R. Kajimoto, H. Yoshizawa, Y. Tomioka, H. Kuwahara, and Y. Tokura, Phys. Rev. Lett. **78**, 4253 (1997).
[8] E. O. Wollan and W. C. Koehler, Phys. Rev. **100**, 545 (1955).
[9] T. Akimoto, Y. Maruyama, Y. Moritomo, A. Nakamura, K. Hirota, K. Ohoyama, and M. Ohashi, Phys. Rev. B **57**, 5594 (1998).
[10] P. D. Battle, M. A. Green, N. S. Laskey, J. E. Millburn, P. G. Radaelli, M. J. Rosseinsky, S. P. Sullivan, and J. F. Vente, Phys. Rev. B **54**, 15 967 (1996).
[11] Y. Moritomo, Y. Maruyama, T. Akimoto, and A. Nakamura, Phys. Rev. B **56**, R7057 (1997).
[12] Y. Moritomo, Y. Maruyama, T. Akimoto, and A. Nakamura, J. Phys. Soc. Jpn. **67**, 405 (1998).
[13] Y. Moritomo, H. Kuwahara, and Y. Tomioka, and Y. Tokura, Phys. Rev. B **55**, 7549 (1997).
[14] F. Izumi, in *The Rietveld Method*, edited by R. A. Young (Oxford University Press, Oxford, 1993), Chap. 13; Y.-I. Kim and F. Izumi, J. Ceram. Soc. Jpn. **102**, 401 (1994).
[15] Low-temperature resistivity measurement indicates that $Nd_{0.45}Sr_{0.55}MnO_3$ is an anisotropic metal with finite conductivity at zero temperature [H. Kuwahara *et al.* (unpublished)].
[16] H. Kuwahara, Y. Moritomo, Y. Tomioka, A. Asamitsu, M. Kasai, R. Kumai, and Y. Tokura, Phys. Rev. B **56**, 9386 (1997).
[17] H. Kawano, R. Kaj'mot, and H. Yoshizara (private communication).